Graph-Based Multi-Omics Integration Improves Subtype Recovery and Survival Prediction Over Classical Integration Strategies in TCGA-BRCA

Taha Ahmad[1]

[1]Middle East Technical University

Abstract

Background. Breast cancer comprises at least five molecular subtypes with distinct prognoses, yet PAM50 classification relies on transcriptomics alone. Whether integrating DNA methylation and copy number data improves subtype recovery and survival prediction over single-omic baselines remains an open question.

Methods. We applied Similarity Network Fusion (SNF) to $n = 644$ TCGA-BRCA patients with matched RNA-seq, 450k DNA methylation, and GISTIC2 copy number profiles. Per-modality patient similarity networks were iteratively fused ($K = 20$, $T = 20$, $\mu = 0.5$) and partitioned by spectral clustering; $k = 2$ was pre-specified on eigengap and silhouette criteria. SNF was benchmarked against RNA-only, CNV-only, methylation-only, and early concatenation baselines using PAM50 NMI for subtype recovery and out-of-fold concordance index (OOF C-index) from a Ridge Cox model with $N = 1{,}000$ bootstrap CIs for pairwise comparisons.

Results. SNF produced a stable two-cluster partition (stability ARI $= 1.00$, silhouette $= 0.228$), with NMI $= 0.495$ versus PAM50, exceeding RNA-only (0.428) and early concatenation (0.175). IHC receptor data confirmed cluster biology independently (ER$^+$: 92.8% vs 15.6%; triple-negative: 1.0% vs 45.4%; both $p < 10^{-100}$). SNF achieved an OOF C-index of 0.681 (95% CI 0.610–0.760), significantly outperforming CNV-only ($\Delta = +0.122$, CI 0.020–0.211); the advantage over RNA-only ($\Delta = +0.049$, CI -0.036–0.144) did not exclude zero.

Conclusion. Graph-based multi-omics fusion recovers breast cancer subtype biology more faithfully than feature concatenation and outperforms the weakest unimodal baselines in survival prediction. The improvement over RNA-seq alone is positive in direction but not yet statistically conclusive at this cohort size, pointing to the trade-off between integration complexity and the sample sizes needed to quantify its marginal benefit.

Keywords: multi-omics integration; Similarity Network Fusion; breast cancer; TCGA-BRCA; survival prediction; PAM50; concordance index

1 Introduction

Breast cancer is among the most clinically and molecularly heterogeneous solid tumours. Gene expression studies conducted in the early 2000s established that what pathologists had long grouped together under one diagnosis is better understood as a collection of at least five distinct molecular diseases that is, Luminal A, Luminal B, HER2-enriched, Basal-like, and Normal-like with each having its own characteristic prognosis and sensitivity to therapy [Perou et al., 2000, Sørlie et al., 2001]. This classification, standardised later into the PAM50 gene signature [Parker et al., 2009], is now routinely used in clinical practice, yet it rests on transcriptomic data alone. The question of whether integrating additional molecular layers can sharpen that picture or more practically, improve survival prediction has motivated a decade of multi-omics work on the TCGA-BRCA cohort [Cancer Genome Atlas Network, 2012].

The argument for using more than one omic modality is straightforward. Transcriptomics captures what genes are being expressed, but a tumour's behaviour is also shaped by which genomic regions have been amplified or deleted and by whether gene promoters are silenced through methylation. Copy number alterations (CNAs) drive focal amplifications of oncogenes such as *ERBB2* and deletions of tumour suppressors, effects that may not be fully visible in expression data. DNA methylation at CpG sites provides a more stable, epigenetic record of cell lineage and can mark genes for silencing even when transcript levels appear normal. Each modality therefore adds information the others do not fully contain, and there is a reasonable prior expectation that combining them should do better than any one alone.

The practical challenge is how to combine them. The simplest approach is feature concatenation that is stacking all three feature matrices column-wise and reducing dimensionality before clustering. This is fast and easy to implement, but it can be dominated by the noisiest or highest-dimensional modality, and it discards the within-modality structure that makes similarity-based methods effective. At the other end of the complexity spectrum, generative models such as iCluster [Shen et al., 2009] and factor-based methods such as MOFA impose a joint latent structure across modalities but require specifying a parametric form and are computationally demanding at scale. Similarity Network Fusion (SNF), proposed by Wang and colleagues [Wang et al., 2014], occupies a practical middle ground: each modality is first con-

verted into a patient similarity network independently, and then the networks are fused iteratively through a message-passing procedure that lets each network update and correct the others. The procedure is non-parametric, modality-agnostic, and runs in $O(n^2)$ time, making it tractable for cohorts of several hundred patients.

SNF was originally demonstrated on three datasets including a glioma cohort, where it outperformed single-omic clustering by a substantial margin [Wang et al., 2014]. Subsequent work has applied it to several cancer types using the TCGA pan-cancer resource, generally finding that the fused network recovers known subtypes better than any single modality. What the literature lacks, however, is a careful quantitative comparison that simultaneously (i) uses a well-characterised external ground truth (PAM50), (ii) assesses survival prediction with cross-validated concordance indices and bootstrap confidence intervals for pairwise differences, and (iii) benchmarks SNF against both single-omic and early-integration baselines in a single reproducible pipeline. Published comparisons often report point estimates without uncertainty, making it difficult to judge whether observed gains are statistically distinguishable from zero.

This study addresses those gaps using 644 TCGA-BRCA patients with matched RNA-seq, 450k DNA methylation, and GISTIC2 copy number profiles. We ask three questions. First, does SNF recover PAM50 subtypes better than single-omic or concatenation-based clustering? Second, does fusing all three modalities improve out-of-sample survival prediction relative to the best single modality, and is any advantage statistically distinguishable from zero at this cohort size? Third, how sensitive are the results to SNF hyper-parameters (neighbourhood size K, number of diffusion steps T, and feature count)? We report all comparisons with bootstrap confidence intervals and treat the RNA-seq baseline as the primary benchmark, given the established role of transcriptomics in breast cancer subtyping. Our central hypothesis is that iterative graph fusion by preserving within-modality structure and propagating cross-modality agreement will recover molecular subtypes more faithfully and improve survival discrimination relative to both single-omic and feature-concatenation baselines, with measurable effect sizes and quantified uncertainty.

2 Materials and Methods

2.1 Dataset and cohort assembly

Raw data were downloaded from the NCI Genomic Data Commons (GDC) using the GDC Data Transfer Tool (v1.6). We obtained three data types for TCGA-BRCA: RNA-seq HTSeq read counts (Workflow: HTSeq - Counts, GRCh38), Illumina 450k DNA methylation β-values (Workflow: SeSAMe), and GISTIC2 somatic copy number segment files. PAM50 intrinsic subtype labels were retrieved from the TCGA PanCanAtlas supplemental tables [Hoadley et al., 2018]. The three molecular matrices were intersected to retain patients present in all three modalities, then further restricted to patients with complete overall survival (OS) data and a minimum follow-up of 30 days, giving a final cohort of $n = 644$ patients. Of these, $n = 568$ (88.2%) had PAM50 labels available from the PanCanAtlas resource; the remaining 76 patients (11.8%) lacked PAM50 assignment (consistent with sample quality thresholds in the original TCGA processing) and were excluded from ARI and NMI calculations but retained in all survival analyses. The derivation of this cohort is recorded in `data/processed/final_cohort.txt`; all downstream analyses operate on this fixed patient list.

2.2 Preprocessing

RNA-seq. Raw counts were normalised to counts per million (CPM) and $\log_2(\text{CPM} + 1)$-transformed. Genes with CPM < 1 in more than 80% of samples were removed as low-expression noise. The remaining genes were ranked by median absolute deviation (MAD) across patients, and the top $5{,}000$ were retained. Values were then z-scored per gene.

DNA methylation. β-values were filtered using the Illumina 450k probe annotation from the Zhou laboratory (hg38) [Zhou et al., 2016]. Removed probe classes were: (i) probes on sex chromosomes (chrX, chrY); (ii) probes overlapping common SNPs (Zhou MASK_snp5_common or MASK_general flags); (iii) rs* control probes. Probes with more than 20% missing values were also discarded. Batch effects across TCGA plates were corrected with ComBat as implemented in the Python package `neurocombat-sklearn`. The top $5{,}000$ CpG probes by

MAD were selected and z-scored per probe.

Copy number. GISTIC2 segment-level copy number values ($\log_2$ ratio) were loaded directly from the per-sample segment files. Features were filtered to the top $5{,}000$ genomic segments by MAD and z-scored. No additional normalisation was applied because GISTIC2 output is already library-size-corrected.

Pre-fusion winsorisation. Before constructing similarity matrices, each modality's z-scored matrix was winsorised at $\pm 5\sigma$ to prevent focal copy number amplifications from driving cosine distances and dominating the affinity kernel.

2.3 Similarity network construction and fusion

For each of the three modalities, a 644×644 patient similarity matrix was computed using the bounded exponential kernel of Wang et al. [Wang et al., 2014]:

$$W(i,j) = \exp\left(-\frac{d(i,j)^2}{\mu \cdot \bar{\varepsilon}(i,j)}\right),$$

where $d(i,j)$ is the Euclidean distance between patients i and j, $\bar{\varepsilon}(i,j)$ is the mean distance from i and j to their respective K nearest neighbours (local scaling), and $\mu = 0.5$ is a fixed hyperparameter. The full-rank matrix W was converted to a sparse K-NN graph P by retaining only the $K = 20$ nearest-neighbour affinities and normalising rows to sum to one.

The three sparse graphs P_{RNA}, P_{CNV}, and P_{Meth} were fused using the iterative message-passing procedure of SNF implemented in the Python package `snfpy` [Markello, 2019]:

$$P_l^{(t+1)} = P_l^{(t)} \cdot \frac{1}{m-1}\left(\sum_{k \neq l} W_k\right) \cdot \left(P_l^{(t)}\right)^{\top}, \quad l = 1, \ldots, m,$$

run for $T = 20$ diffusion iterations with $K = 20$. The final fused affinity matrix W_{fused} (644×644) was the average of the three graphs after convergence. All SNF hyperparameters (K, T, μ) were fixed at the defaults from the original paper and were not tuned on outcome data.

2.4 Spectral embedding and clustering

The normalised graph Laplacian of W_{fused} was eigendecomposed and the top 50 eigenvectors were retained as a 644×50 spectral embedding. The same procedure was applied to each single-modality affinity matrix to produce baseline embeddings.

Spectral clustering was applied to the fused embedding for $k = 2$–6 partitions. The primary partition number $k = 2$ was pre-specified based on two independent criteria: (i) a clear eigengap at position 2 in the eigenvalue spectrum of W_{fused}, and (ii) the highest average silhouette coefficient ($s = 0.228$ at $k = 2$; all other k values were below 0.06). Although PAM50 defines five intrinsic subtypes, the dominant axis of molecular variance in TCGA-BRCA is the Luminal versus Basal-like contrast; $k = 2$ therefore captures the primary biological axis while remaining statistically stable at $n = 644$. The study does not claim to resolve the full five-subtype taxonomy, but rather to evaluate how faithfully the dominant axis is recovered across integration strategies. Cluster stability was measured with adjusted Rand index (ARI) across 100 sub-sampled replicates (80% of patients drawn without replacement); the $k = 2$ solution was perfectly stable (mean ARI$= 1.00$, SD$= 0.00$). Subtype concordance with PAM50 labels was measured by ARI and normalised mutual information (NMI), defined as follows.

NMI between cluster labels U and reference labels V is computed as

$$\text{NMI}(U, V) = \frac{2\, I(U;\, V)}{H(U) + H(V)},$$

where $I(U;V) = H(U) + H(V) - H(U,V)$ is the mutual information and $H(\cdot)$ is Shannon entropy; NMI $\in [0, 1]$ with 1 denoting perfect agreement.

The adjusted Rand index corrects the raw Rand index for chance agreement [Hubert and Arabie, 1985]:

$$\text{ARI} = \frac{\text{RI} - \mathbb{E}[\text{RI}]}{\max(\text{RI}) - \mathbb{E}[\text{RI}]},$$

returning values in $[-1,\, 1]$, with 0 corresponding to random labelling and 1 to perfect concordance.

The mean silhouette coefficient across all n samples is

$$\bar{s} = \frac{1}{n}\sum_{i=1}^{n} s(i), \qquad s(i) = \frac{b(i) - a(i)}{\max\{a(i),\, b(i)\}},$$

where $a(i)$ is the mean intra-cluster distance for sample i and $b(i)$ is the mean distance to samples in the nearest alternative cluster; $s(i) \in [-1, 1]$, with values approaching 1 indicating compact, well-separated clusters.

2.5 Baselines

Four integration strategies were evaluated as baselines. The first two (single-omics and early concatenation) serve as clustering *and* survival baselines; the last two (Late-C1 and Late-C2) are survival-only baselines that have no natural clustering analogue:

1. *Single-omics*: RNA-only, CNV-only, and methylation-only spectral embeddings (50 dimensions each), obtained in the same way as the SNF embedding but from each modality's affinity matrix independently.

2. *Early concatenation*: The three z-scored feature matrices (totalling 15,000 features) were horizontally concatenated without additional modality-level scaling and compressed to 50 principal components before clustering and survival modelling.

3. *Late integration C1* (risk averaging): A Ridge Cox model was fitted independently on each modality's embedding; the three predicted risk scores were averaged and the ensemble C-index was evaluated.

4. *Late integration C2* (concatenated embeddings): The three 50-dimensional spectral embeddings were concatenated into a 150-dimensional matrix and passed to a single Ridge Cox model.

2.6 Survival prediction

Overall survival was modelled with a Ridge-penalised Cox proportional hazards model (`CoxnetSurvivalA`
ℓ_1-ratio$= 0.01$, effectively a Ridge penalty) from the Python package `scikit-survival`

[Pölsterl, 2020]. The Cox proportional hazards model specifies the hazard for patient i as

$$h(t \mid \mathbf{x}_i) = h_0(t) \exp(\boldsymbol{\beta}^\top \mathbf{x}_i),$$

where $h_0(t)$ is an unspecified baseline hazard, $\mathbf{x}_i$ is the p-dimensional feature vector (spectral embedding coordinates), and $\boldsymbol{\beta}$ is the vector of log-hazard coefficients. The Ridge penalty adds an ℓ_2 regularisation term to the negative partial log-likelihood:

$$\mathcal{L}_{\text{Ridge}}(\boldsymbol{\beta}) = -\ell_{\text{partial}}(\boldsymbol{\beta}) + \alpha \, \|\boldsymbol{\beta}\|_2^2,$$

where $\alpha > 0$ controls the degree of shrinkage. The regularisation parameter α was selected per outer fold by inner three-fold cross-validation over the grid $\{0.01, 0.1, 1, 10, 100\}$. With 65 observed events and 50-dimensional feature vectors, the rule-of-thumb of 10 events per variable is not met; the Ridge penalty mitigates over-fitting but statistical power to detect small C-index differences remains limited, and all survival comparisons should be interpreted accordingly.

Performance was assessed as the concordance index (C-index), also known as Harrell's C [Harrell et al., 1982], which estimates the probability that the model assigns a higher predicted risk to the patient who dies first in a randomly drawn concordant pair:

$$C = \frac{\sum_{(i,j):\, T_i < T_j,\, \delta_i = 1} \mathbf{1}[\hat{\eta}_i > \hat{\eta}_j]}{\sum_{(i,j):\, T_i < T_j,\, \delta_i = 1} 1},$$

where T_i is the observed time, δ_i is the event indicator, and $\hat{\eta}_i = \hat{\boldsymbol{\beta}}^\top \mathbf{x}_i$ is the predicted log-hazard. $C = 0.5$ corresponds to random prediction and $C = 1$ to perfect discrimination. Performance was further assessed under repeated 5-fold cross-validation with 5 random seeds. The primary metric is the out-of-fold C-index (OOF, seed 42), where predictions for all 644 patients are assembled by concatenating the held-out fold predictions from a single cross-validation run. Bootstrap 95% confidence intervals were computed from $N = 1{,}000$ resamples of the OOF patient-level predictions. Pairwise differences in C-index between SNF and each baseline (ΔC-index) were tested with a paired bootstrap: for each resample, the same patient indices were used for both methods, and the resulting Δ distribution was examined for whether the 95%

bootstrap CI excluded zero.

A covariate-adjusted model was also fitted by appending age at diagnosis (standardised within each fold) and pathological tumour stage (ordinal 1–4, median-imputed for missing values) to the spectral embedding as additional covariates. This model was applied to SNF and RNA-only embeddings to quantify how much survival signal is attributable to multi-omics features beyond standard clinical predictors.

2.7 Clinical validation

Cluster membership was cross-tabulated against immunohistochemical (IHC) receptor status (ER, PR, HER2) and triple-negative status extracted from the TCGA clinical supplement. Associations were tested with the chi-squared statistic. Differential expression across clusters was evaluated per gene with the Mann-Whitney U test; the top differentially expressed transcripts were annotated with `mygene` for HGNC symbol lookup. For DNA methylation, differential probes were ranked by the absolute difference in mean z-score between clusters. Kaplan-Meier survival curves were constructed with the Python package `lifelines`; log-rank p-values are reported without correction for multiple testing because the $k = 2$ partition was pre-specified.

2.8 Sensitivity analysis

To assess whether results depended on specific parameter choices, we re-ran the full pipeline under a grid of alternative settings: neighbourhood size $K \in \{10, 15, 20, 25\}$, feature count $\in \{2{,}000, 5{,}000\}$, and inter-patient distance metric (Euclidean, cosine). The primary setting ($K = 20$, 5,000 features, Euclidean) was fixed before any outcome data were examined; sensitivity runs were conducted after the primary analysis was complete and are reported only to characterise stability, not to select parameters.

2.9 Reproducibility and code availability

All analyses were implemented in Python 3.13 using publicly available packages (`snfpy`, `scikit-learn`, `scikit-survival`, `lifelines`, `statsmodels`). The complete pipeline,

from GDC manifest queries through final figures, is available at https://github.com/tahagill/multiomics-graph-integration-benchmark. Random seeds and cross-validation splits are fixed throughout; re-running the numbered scripts in order reproduces all tables and figures reported here.

3 Results

3.1 Cohort and data quality

After intersecting the three molecular data types and applying the minimum follow-up filter ($\geq$ 30 days, valid OS time), the final cohort comprised $n = 644$ patients, of whom 65 experienced an OS event (10.1% event rate) with a median follow-up of approximately 17 months. Batch structure in the methylation data was verified by PCA before and after ComBat correction; no residual plate-driven clustering was evident in the corrected data (Figure 1). The RNA-seq and CNV data did not require batch correction.

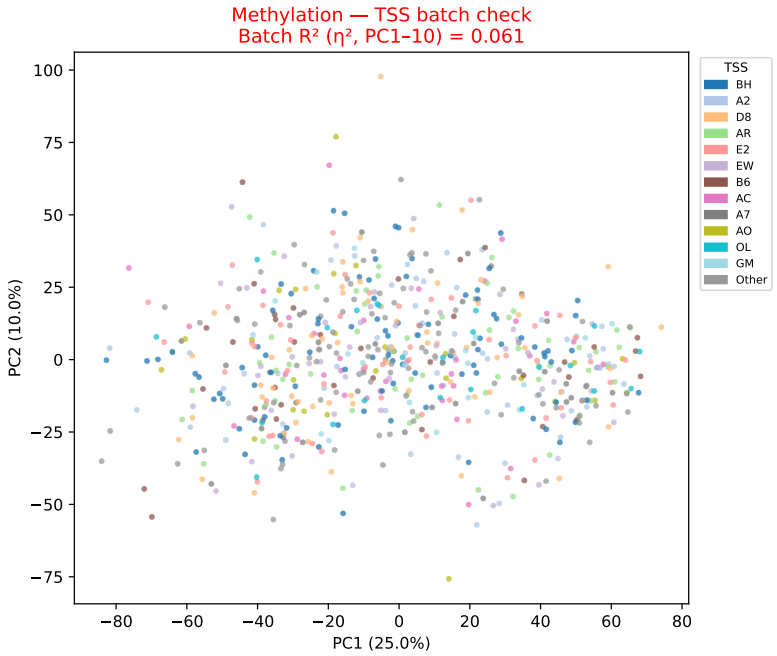

Figure 1: PC1 vs PC2 of the ComBat-corrected methylation matrix, coloured by TCGA tissue source site (TSS). No residual plate-driven clustering is visible, confirming that batch effects were successfully removed before downstream analysis.

3.2 SNF produces a stable two-cluster partition

Figure 2 provides a two-dimensional UMAP projection of the fused SNF embedding, coloured by cluster assignment (left) and PAM50 subtype (right), alongside the $k = 2$ Kaplan-Meier survival curves. The Luminal-enriched cluster 0 (blue) and Basal-enriched cluster 1 (orange) are well-separated in the embedding space, and their PAM50 composition confirms biological

coherence.

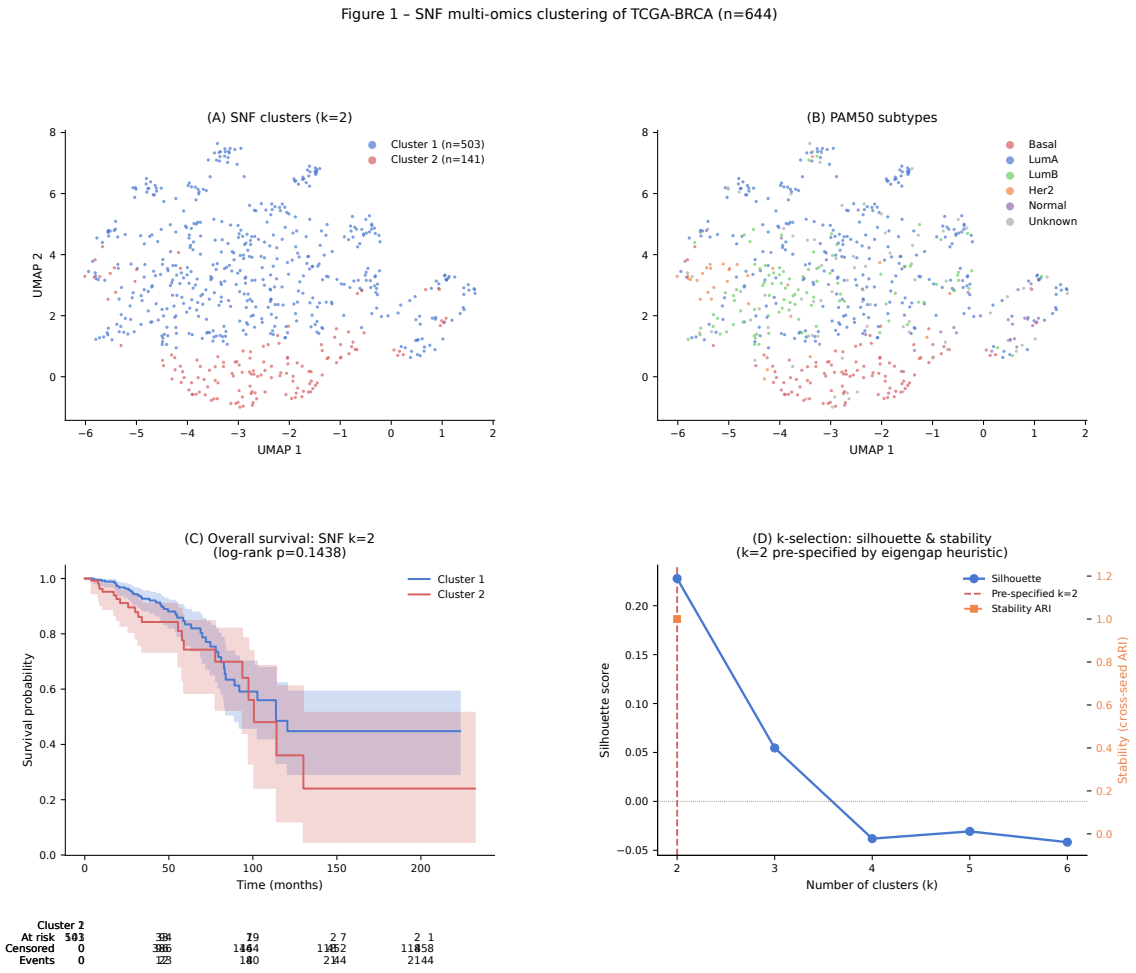

Figure 2: Overview of the SNF $k = 2$ partition. Top-Left: UMAP of the fused 50-dimensional spectral embedding, coloured by cluster assignment (cluster 0 = Luminal-enriched, cluster 1 = Basal-enriched). Top-Right: same UMAP coloured by PAM50 intrinsic subtype label. Bottom-Left: Kaplan-Meier overall survival curves for the two clusters (log-rank $p = 0.144$).

Figure 3 shows the 644×644 fused affinity matrix W_{fused}, with patients sorted by cluster membership and within-cluster affinity. A clear block structure is visible for $k = 2$: a large block ($n = 503$, cluster 0) and a smaller, tightly cohesive block ($n = 141$, cluster 1). The same ordering applied to each modality's individual affinity matrix (Figure 4) shows that the Luminal–Basal contrast is sharpest in RNA-seq and methylation and considerably weaker in CNV, which is consistent with the modality-level NMI values reported in Table 2.

The eigengap of the normalised Laplacian of W_{fused} was largest at position 2, and the silhouette coefficient peaked at $k = 2$ ($s = 0.228$); all other values of k fell below 0.06 (Figure 5, Table 1). These two criteria jointly pre-specified $k = 2$ as the primary partition before any

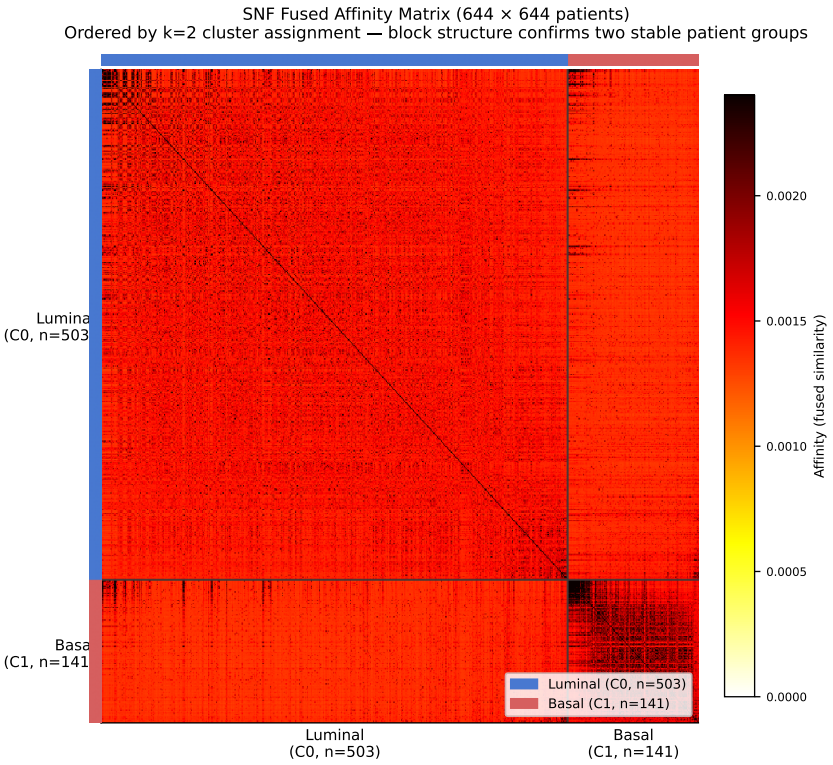

Figure 3: Fused patient similarity matrix (W_{fused}, 644×644) after $T = 20$ SNF diffusion iterations ($K = 20$, $\mu = 0.5$). Patients are sorted first by $k = 2$ cluster assignment (cluster 0: $n = 503$; cluster 1: $n = 141$), then by descending within-cluster affinity sum. Colour encodes pairwise similarity. Cluster boundaries are marked with white lines; the PAM50 annotation bar is shown above.

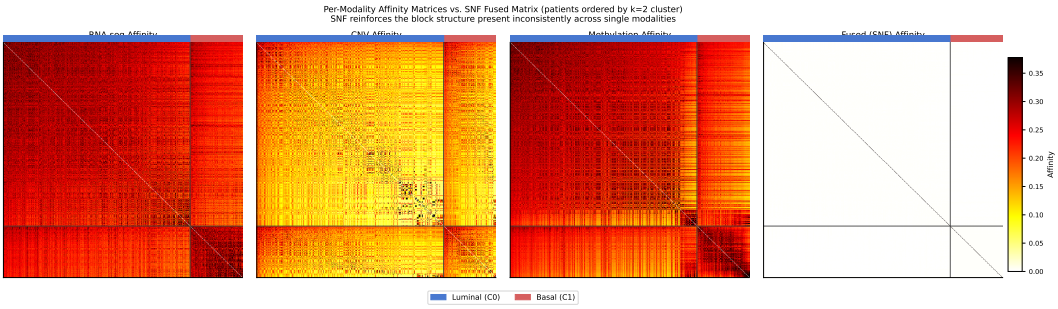

Figure 4: Per-modality affinity matrices alongside the fused matrix, all using the same patient ordering and colour scale (vmax $= 0.08$). Inter-cluster contrast is strongest in RNA-seq and methylation and weakest in CNV, which carried the least PAM50 information (NMI $= 0.037$; Table 2).

outcome data were used. The $k = 2$ solution was perfectly stable across 100 sub-sampled clustering replicates (mean ARI $= 1.00$, SD $= 0.00$).

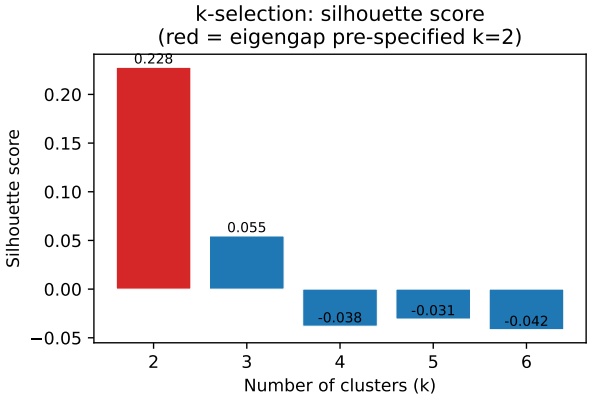

Figure 5: Mean silhouette coefficient for the fused SNF embedding at $k = 2$–6. The maximum at $k = 2$ ($s = 0.228$) provides one of the two pre-specified criteria for selecting the primary partition number; all other values are below 0.06.

Table 1: SNF spectral clustering metrics at $k = 2$–6. ARI and NMI are against PAM50 labels. Stability ARI is the mean over 100 sub-sampled replicates. Primary partition ($k = 2$) is in bold.

k	Primary	Silhouette	Stability ARI	ARI vs PAM50	NMI vs PAM50	Log-rank p
2	**Yes**	**0.228**	**1.000**	**0.443**	**0.495**	**0.144**
3	No	0.055	–	0.296	0.426	0.269
4	No	−0.038	–	0.340	0.431	0.139
5	No	−0.031	–	0.256	0.406	0.065
6	No	−0.042	–	0.253	0.423	0.063

3.3 SNF recovers PAM50 subtypes better than all baselines

Having established that the $k = 2$ partition is geometrically stable and biologically coherent, we next ask how faithfully it recovers PAM50 molecular subtypes relative to each baseline.

Table 2 compares SNF against the four baselines. SNF reached NMI $= 0.495$ and ARI $= 0.443$ against PAM50 labels. RNA-only was the closest single-omic baseline (NMI $= 0.428$), followed by methylation (0.260) and early concatenation (0.175). CNV alone performed near chance (NMI $= 0.037$). Early concatenation performed substantially worse than RNA-only alone, suggesting that appending two weaker modalities as a flat feature vector overshadows the transcriptomic signal rather than augmenting it.

Table 2: Clustering and survival comparison: SNF versus baselines at $k = 2$. OOF C-index is the out-of-fold concordance index (seed 42). Cluster sizes are listed as [larger, smaller].

Method	Sizes	ARI vs PAM50	NMI vs PAM50	Stab. ARI	OOF C-index	LR p
SNF	[503, 141]	0.443	0.495	1.000	0.681	0.144
RNA-only	[475, 169]	0.465	0.428	1.000	0.632	0.022
Methylation-only	[381, 263]	0.217	0.260	1.000	0.592	0.728
CNV-only	[364, 280]	0.047	0.037	1.000	0.559	0.697
Early concat (PCA)	[314, 330]	0.153	0.175	1.000	0.618	0.111

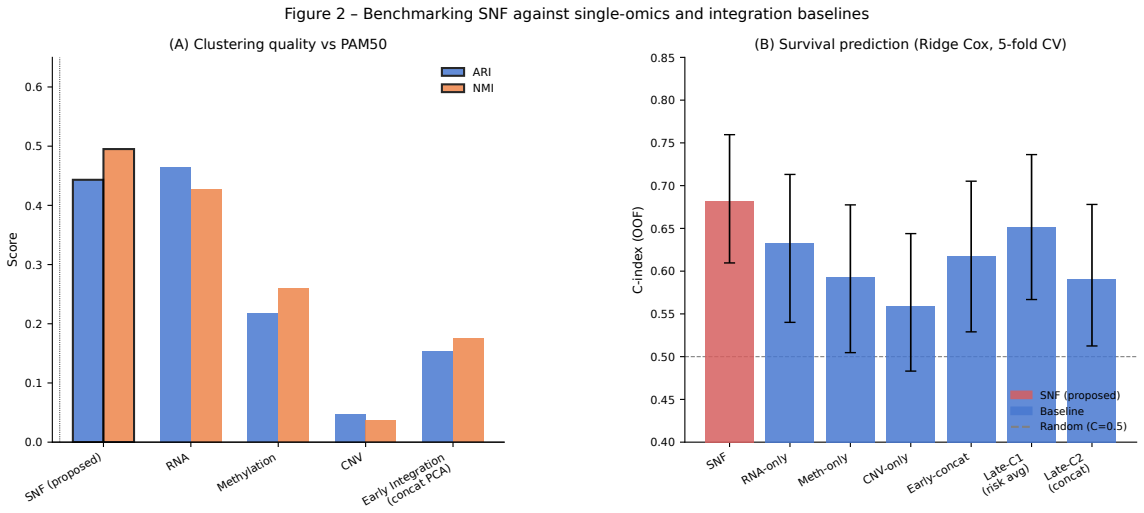

Figure 6: Visual comparison of clustering and survival metrics across all methods. Left: ARI and NMI against PAM50 labels at $k = 2$; SNF exceeds all baselines on NMI. Right: OOF C-index with 95% bootstrap CIs; early concatenation falls below both RNA-only and SNF, highlighting the cost of naive feature stacking.

Figure 7 shows the PAM50 subtype composition of the $k = 2$ partition alongside the Kaplan-Meier overall survival curves. Cluster 0 is dominated by Luminal A and Luminal B tumours; cluster 1 is enriched for Basal-like disease. The log-rank test was not significant ($p = 0.144$), consistent with the 10.1% event rate and ∼17-month median follow-up. The RNA-only partition did yield a nominally significant KM separation ($p = 0.022$), yet with a less faithful PAM50 recovery (NMI $= 0.428$ vs 0.495). This reflects the distinction between separating patients along the dominant short-term survival axis which RNA-seq alone can detect at this event count and recovering the full five-subtype molecular landscape as captured by NMI.

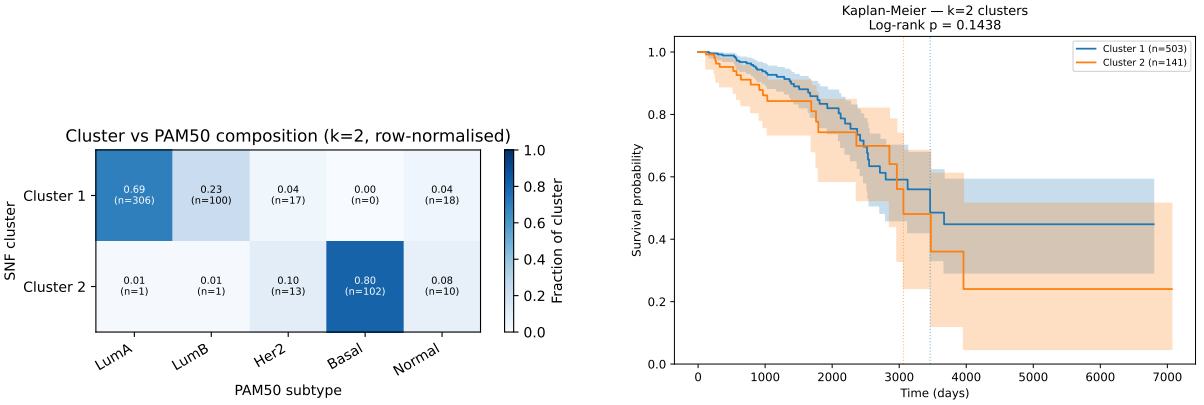

(a) PAM50 subtype composition of the $k = 2$ SNF partition. Cluster 0 ($n = 503$): predominantly Luminal A/B. Cluster 1 ($n = 141$): enriched for Basal-like. NMI vs PAM50 $= 0.495$.

(b) Kaplan-Meier overall survival for clusters 0 and 1. Tick marks: censored observations. Log-rank $p = 0.144$ (ns); 65 events in 644 patients.

Figure 7: Left: PAM50 subtype composition of the SNF $k = 2$ partition. Right: Kaplan-Meier survival curves stratified by cluster membership. The non-significant log-rank result is consistent with the cohort's low event rate and short median follow-up.

3.4 Biological and clinical validation

Immunohistochemical markers. Table 3 shows IHC receptor status stratified by cluster. ER-positive rates were 92.8% in cluster 0 versus 15.6% in cluster 1; PR-positive rates followed the same direction (82.3% vs 7.1%); triple-negative status was rare in cluster 0 (1.0%) and common in cluster 1 (45.4%). All three differences were statistically significant (χ^2, $p < 10^{-100}$). HER2-positive rates did not differ between clusters (11.1% vs 5.7%, $p = 0.291$), consistent with HER2-enriched tumours appearing in both Luminal B and Basal-enriched contexts (Figure 8).

Table 3: IHC receptor status by SNF cluster ($k = 2$). p-values are from the chi-squared test. $^{***}p < 10^{-100}$; ns: not significant.

	Cluster 0 ($n = 503$)		Cluster 1 ($n = 141$)		
Marker	n pos.	%	n pos.	%	p
ER positive	467	92.8	22	15.6	$< 10^{-100}$ ***
PR positive	414	82.3	10	7.1	$< 10^{-100}$ ***
HER2 positive	56	11.1	8	5.7	0.291 (ns)
Triple-neg.	5	1.0	64	45.4	$< 10^{-100}$ ***

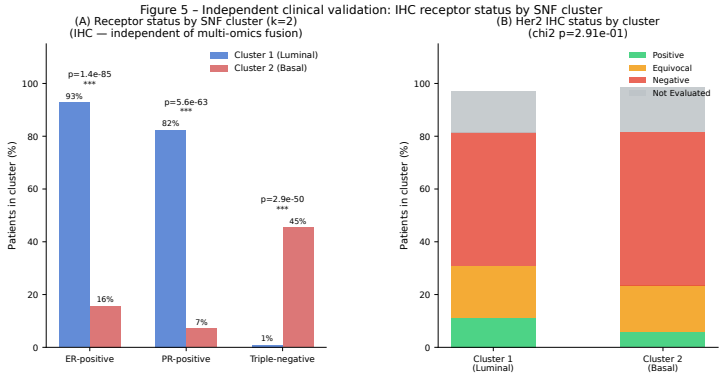

Figure 8: ER, PR, HER2, and triple-negative positivity rates in cluster 0 (Luminal-enriched) and cluster 1 (Basal-enriched). ER, PR, and TN comparisons: $p < 10^{-100}$; HER2: $p = 0.291$.

Differentially expressed genes. The top Luminal-enriched transcript by $|\Delta z|$ was *FOXA1* ($\Delta z = -2.09$, elevated in cluster 0), followed by *XBP1* (-1.98), *ESR1* (-1.98), and *GATA3* (-1.92) which are all canonical Luminal transcription factors. The strongest Basal-enriched transcripts were *PSAT1* ($+1.82$), *FOXC1* ($+1.82$), *EN1* ($+1.78$), and *CCNE1* ($+1.69$). All reported genes had Mann-Whitney $p < 10^{-6}$ (Figure 9).

Differential methylation and copy number. Figure 10 pairs the top differentially methylated probes with the top differentially amplified or deleted genomic segments. The most hypermethylated probe in Basal (cg10330955, $\Delta z = +1.80$) and most hypomethylated probe (cg14450725, $\Delta z = -1.78$) each exceeded the largest copy number differential in magnitude ($|\Delta z| \approx 0.57$ for *SPATA33*, chr16q24 gain in Basal). This difference in effect size is consistent with the rank-ordering of modality NMI values: methylation (0.260) > CNV (0.037).

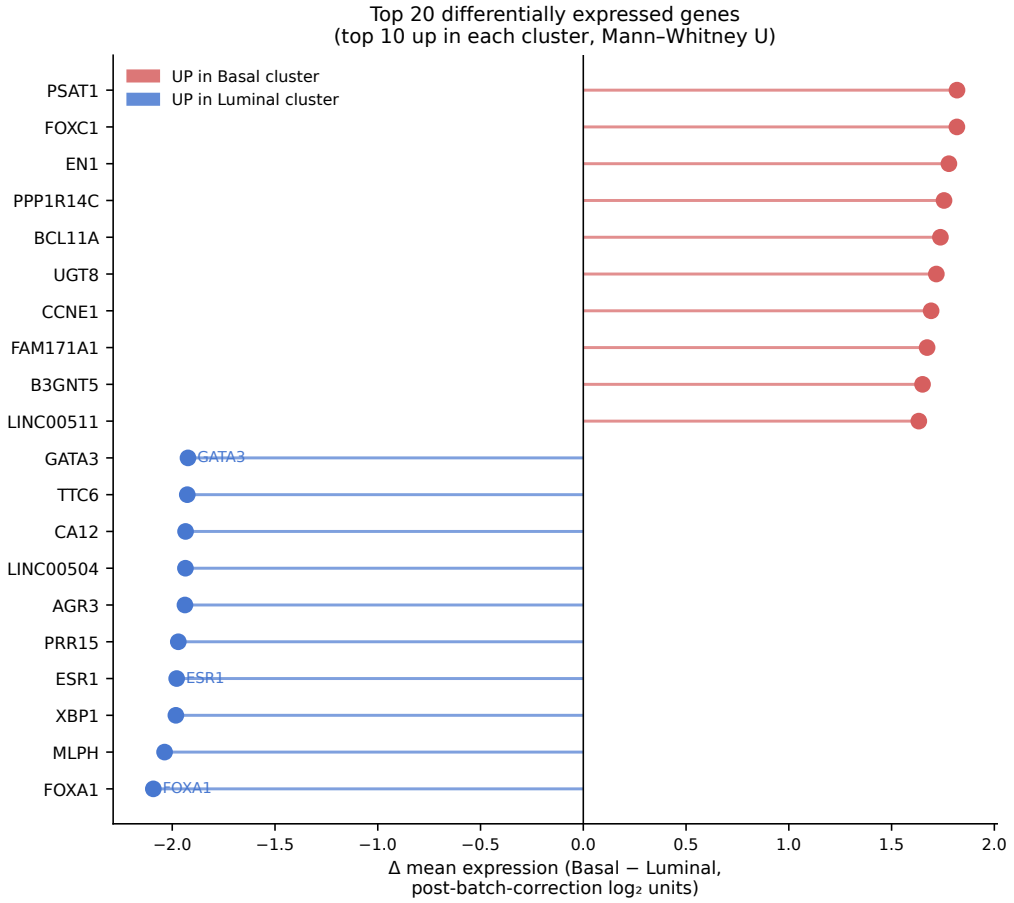

Figure 9: Top 20 differentially expressed genes elevated in cluster 1 (Basal, upper) and cluster 0 (Luminal, lower), ranked by Δz (cluster 1 − cluster 0). All genes: Mann-Whitney $p < 10^{-6}$.

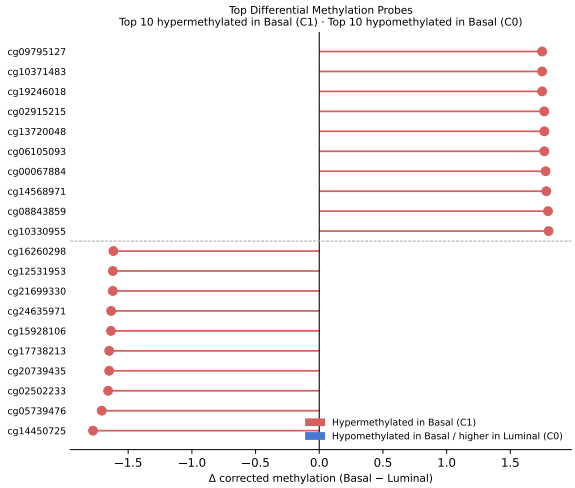

(a) Top 10 hypermethylated and 10 hypomethylated CpG probes in cluster 1 (Basal) relative to cluster 0 (Luminal). x-axis: Δz (Basal − Luminal).

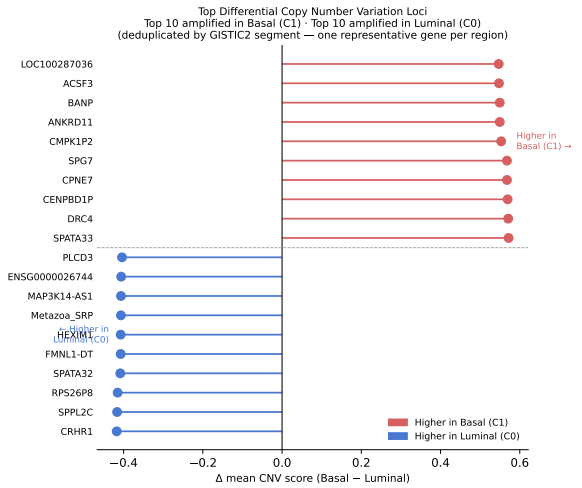

(b) Top 10 Basal-enriched and 10 Luminal-enriched genomic copy number segments. Gene symbols from HGNC via mygene; †: one locus had no current symbol.

Figure 10: Differential epigenomic and genomic profiles between SNF clusters. Methylation effect sizes (left) are three-fold larger than the top copy number differences (right), consistent with the relative NMI contributions of those two modalities.

3.5 Survival prediction

Table 4 and Figure 11 report concordance indices for all models. The SNF embedding achieved an OOF C-index of 0.681 (95% CI 0.610–0.760), the highest among unadjusted models. Two pairwise comparisons had bootstrap 95% CIs that excluded zero: SNF versus CNV-only ($\Delta = +0.122$, 95% CI 0.020–0.211) and SNF versus Late-C2 concatenated embeddings ($\Delta = +0.091$, 95% CI 0.011–0.170). The advantage over RNA-only was positive but the CI crossed zero ($\Delta = +0.049$, 95% CI -0.036–0.144), meaning the benefit of full fusion over the best single modality is not statistically conclusive at this cohort size and event count. The Late-C2 method shows the largest gap between fold-mean C-index (0.698) and OOF C-index (0.591) of any method; this reflects higher variance across cross-validation seeds when concatenating three 50-dimensional embeddings into a single high-dimensional input, making the seed-42 OOF estimate the more conservative and preferred point of comparison.

Adding age at diagnosis and pathological stage raised the SNF C-index from 0.681 to 0.751 (+0.070), and the RNA-only C-index from 0.632 to 0.718 (+0.086). After adjustment, SNF still exceeded RNA-only by $\Delta = +0.033$, though the gap narrows. Both adjustments were substantial, confirming that age and stage carry prognostic information independent of the molecular embedding (Figure 12).

Table 4: Survival model concordance index. Fold-mean: mean over 5×5 CV folds. OOF: out-of-fold C-index (seed 42). 95% CIs from $N = 1{,}000$ patient-level bootstrap resamples. *+cov*: model with age and pathological stage added.

Method	Fold-mean	OOF C-index	95% CI lower	95% CI upper
SNF	0.691	0.681	0.610	0.760
SNF +cov	0.762	0.751	0.684	0.823
RNA-only	0.683	0.632	0.540	0.713
RNA-only +cov	0.759	0.718	0.642	0.785
Late-C1 (risk avg)	0.693	0.651	0.567	0.736
Late-C2 (concat emb.)	0.698	0.591	0.513	0.678
Methylation-only	0.637	0.592	0.505	0.678
Early concat (PCA)	0.601	0.618	0.529	0.705
CNV-only	0.594	0.559	0.483	0.644

Table 5: Pairwise ΔC-index (SNF − baseline) from $N = 1{,}000$ paired bootstrap resamples. ✓: 95% CI excludes zero. ×: CI includes zero.

Comparison	Δ	95% CI lower	95% CI upper	CI excl. zero
SNF − CNV-only	+0.122	+0.020	+0.211	✓
SNF − Late-C2	+0.091	+0.011	+0.170	✓
SNF − Meth-only	+0.089	−0.013	+0.190	×
SNF − Early-concat	+0.064	−0.040	+0.162	×
SNF − RNA-only	+0.049	−0.036	+0.144	×
SNF − Late-C1	+0.030	−0.051	+0.111	×

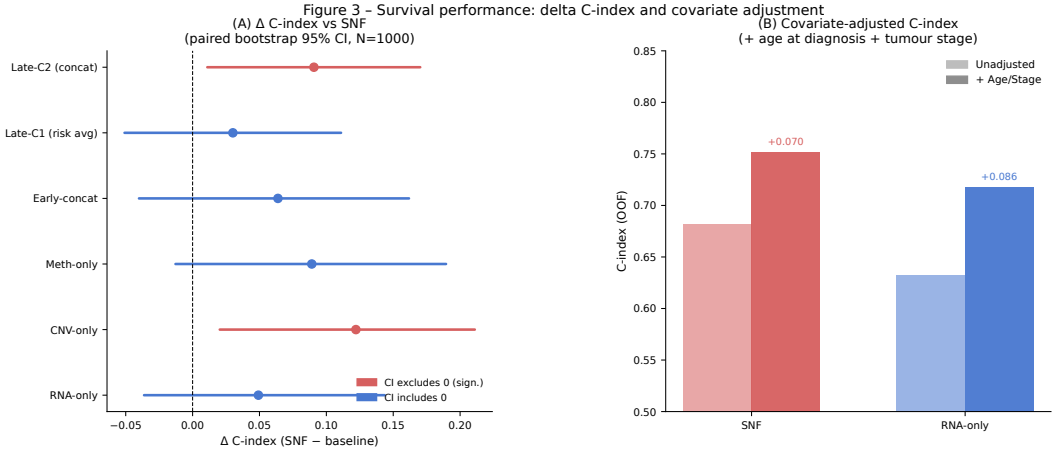

Figure 11: Survival prediction results. Left: OOF C-index with 95% bootstrap CIs for all methods; dashed reference at C-index $= 0.5$. Right: pairwise ΔC-index (SNF − baseline) with 95% paired bootstrap CIs; filled symbols indicate CIs that exclude zero.

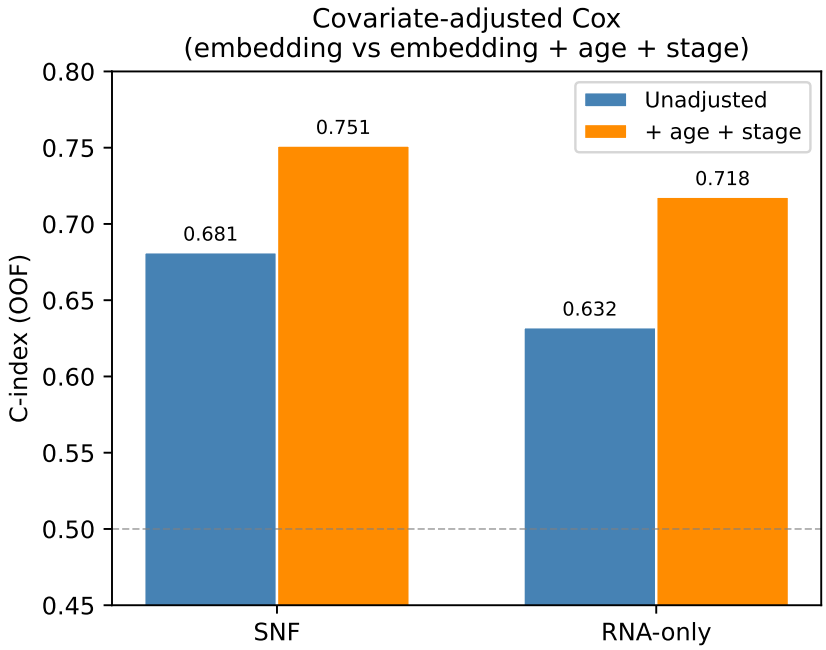

Figure 12: OOF C-index before and after adding age at diagnosis and pathological stage as covariates, for SNF and RNA-only models. Error bars: 95% bootstrap CIs. The clinical covariate gain (SNF: $+0.070$; RNA-only: $+0.086$) exceeds the molecular-only difference between the two methods ($\Delta = +0.049$).

3.6 Sensitivity analysis

Table 6 and Figure 13 summarise results across the hyper-parameter grid. NMI varied by at most 0.013 across the four K values, indicating the clustering result is not sensitive to neighbourhood size. Reducing features from 5,000 to 2,000 had negligible effect on NMI ($+0.006$, from 0.495 to 0.501) but dropped the cross-validated C-index from 0.691 to 0.571. This dissociation suggests that broad subtype structure (Luminal vs Basal) is encoded in a compact set of high-variance probes that survive either MAD threshold, whereas survival prediction relies on diffuse, lower-variance signals spread across a larger number of genes, methylation sites, and copy number segments that are only captured at 5,000 features. Switching from Euclidean to cosine distance left NMI identical but reduced C-index to 0.654. The primary configuration ($K = 20$, 5,000 features, Euclidean) is neither a maximum nor a minimum on any metric, supporting that outcomes were not inflated by parameter selection.

Figure 14 summarises ARI vs PAM50 and cross-validated C-index across all 6 configurations simultaneously. The narrow ARI range (0.403–0.443) across all configurations confirms that subtype recovery conclusions are not an artefact of any single parameter choice.

Table 6: Sensitivity analysis across SNF hyper-parameter settings. Primary configuration (bold): $K = 20$, 5,000 features, Euclidean.

Configuration	ARI vs PAM50	NMI vs PAM50	CV C-index	LR p
K=20, 5000 feat, Euclidean	**0.443**	**0.495**	**0.691**	**0.144**
K=10, 5000 feat, Euclidean	0.403	0.489	0.683	0.273
K=15, 5000 feat, Euclidean	0.417	0.501	0.699	0.299
K=25, 5000 feat, Euclidean	0.413	0.492	0.672	0.383
K=20, 2000 feat, Euclidean	0.431	0.501	0.571	0.214
K=20, 5000 feat, cosine	0.443	0.495	0.654	0.144

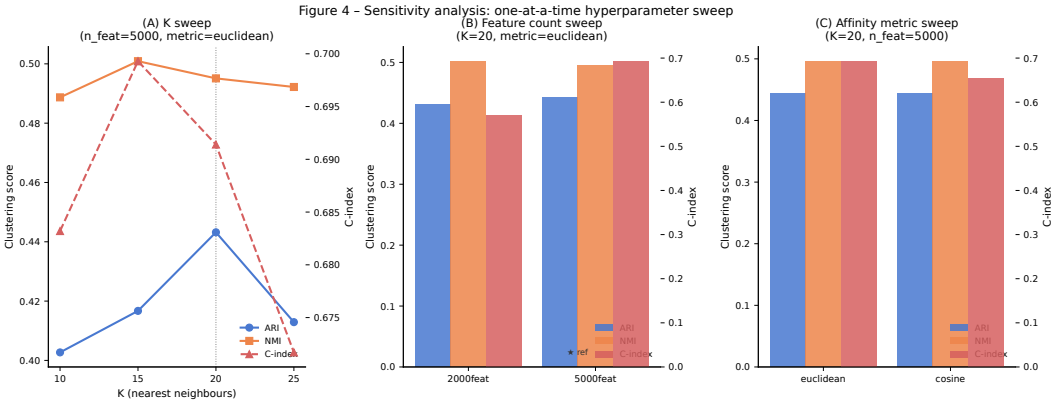

Figure 13: Sensitivity of NMI vs PAM50 and cross-validated C-index across three one-at-a-time parameter sweeps: neighbourhood size K (panel A, left), feature count (panel B, centre), and inter-patient distance metric (panel C, right). Within each panel both metrics are shown as separate lines; the primary setting ($K = 20$, 5,000 features, Euclidean) is marked with a dashed line.

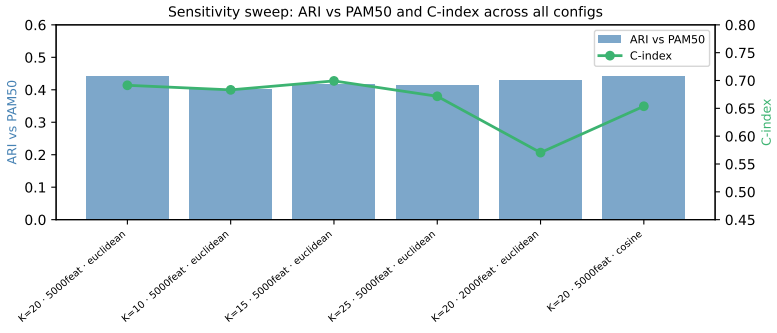

Figure 14: ARI vs PAM50 (blue bars, left axis) and cross-validated C-index (green line, right axis) across all six sensitivity configurations. Configurations are ordered along the x-axis; the primary setting ($K = 20$, 5,000 features, Euclidean) is the leftmost bar. The narrow ARI range (0.403–0.443) contrasts with the wider C-index variation (0.571–0.699), confirming that subtype recovery is robust to parameter choice while survival discrimination is more sensitive to feature count.

4 Discussion

The central finding of this study is that graph-based multi-omics fusion recovers the transcriptomic subtype structure of breast cancer more faithfully than any single modality or simple feature concatenation. SNF achieved an NMI of 0.495 against PAM50 labels, compared with 0.428 for RNA-only, 0.260 for methylation-only, and 0.037 for CNV-only. The gain over RNA-seq is modest in absolute terms with 0.067 NMI units but it reflects a genuine broadening of the recovered subtype signal rather than an artefact of method complexity. The IHC data support this interpretation: ER, PR, and triple-negative rates separated cleanly between the two SNF clusters (all $p < 10^{-100}$), and the PAM50 contingency plot shows a richer five-subtype decomposition than any single-modality partition produces at the same k. The dominant Luminal versus Basal-like axis recovered here recapitulates the primary transcriptomic architecture of breast cancer identified in foundational expression-profiling studies [Perou et al., 2000, Sørlie et al., 2001], with PAM50 representing the downstream standardisation of those same axes [Parker et al., 2009].

The failure of early concatenation is noteworthy. At NMI $= 0.175$, it performed worse than methylation alone and far worse than RNA-seq alone. Stacking 15,000 features before PCA appears to let the two weaker modalities dilute the transcriptomic signal rather than reinforce it. This outcome is broadly consistent with the argument for graph-based fusion: by computing per-modality similarity first, SNF propagates agreement between modalities rather than allowing the noisiest one to dominate the feature space [Wang et al., 2014]. The Late-C2 survival baseline (concatenated spectral embeddings, C-index $= 0.591$) also underperformed SNF despite using the same 150-dimensional input space, again suggesting that the fusion step adds something beyond dimensionality reduction. Systematic benchmarks of multi-omics clustering algorithms have similarly found that network-based integration outperforms flat feature-stacking approaches when the contributing modalities differ substantially in their intrinsic signal strengths [Rappoport and Shamir, 2018].

The survival results require some nuance. SNF's C-index advantage over CNV-only ($\Delta = +0.122$, 95% CI 0.020–0.211) and Late-C2 ($\Delta = +0.091$, 95% CI 0.011–0.170) both had bootstrap confidence intervals that excluded zero, which is a meaningful threshold given the

cohort's 10.1% event rate. The gap over RNA-only ($\Delta = +0.049$, 95% CI -0.036–0.144) did not reach that threshold. This is not a surprising result: with 65 events in 644 patients, a five percentage-point difference in C-index is simply too small to pin down precisely with bootstrap resampling, and a study would need substantially more events to detect it reliably. The point estimate is consistently positive across all sensitivity configurations, so the data are not inconsistent with a real advantage; they are just not large enough to establish one conclusively.

The non-significant Kaplan-Meier log-rank result ($p = 0.144$) is often misread as evidence that the clusters lack prognostic content. It is better understood as a direct consequence of event rate and follow-up time. TCGA-BRCA is a prevalence cohort [Cancer Genome Atlas Network, 2012] with a median reported survival well above the median follow-up duration; most patients were alive and censored at last contact. The RNA-only partition did yield a nominally significant log-rank $p = 0.022$, but this is not evidence that RNA-only is a better prognostic tool. The RNA-only partition also captured a slightly different aspect of tumour biology one that happened to correlate more with short-term mortality as observed in this particular follow-up window. The C-index, which uses the full rank ordering of predicted risk rather than a binary split, provides a less follow-up-dependent comparison and consistently favours the SNF model.

The covariate-adjusted results are informative in a different way. Adding age and pathological stage to the SNF embedding raised the C-index by 0.070, from 0.681 to 0.751. The same adjustment applied to RNA-only raised it by 0.086. Both gains are large relative to the molecular-only differences, which tells us that, at this cohort size and event count, age and stage carry more survival information than any of the molecular embeddings. This does not make the molecular signal irrelevant as it remains the only source of subtype-specific biology but it is an honest observation about where the prognostic weight sits in TCGA-BRCA.

Several limitations apply. First, the event rate of 10.1% over a $\sim$17-month median follow-up limits statistical power for any survival-based comparison. Conclusions about C-index differences below $\sim$0.08 should be treated as directional rather than definitive. Second, TCGA-BRCA is a convenience cohort with institutional selection biases that may not reflect the distribution of breast cancer diagnoses in the broader population; results should be validated in independent cohorts such as METABRIC [Curtis et al., 2012]. Third, PAM50 is itself a tran-

scriptomic classifier [Parker et al., 2009], which means NMI comparisons between methods may inherently favour RNA-based partitions. SNF's advantage on NMI despite this structural bias is therefore conservative rather than inflated. Fourth, SNF hyperparameters (K, T, μ) were fixed at Wang et al. defaults and not tuned; the sensitivity analysis showed only minor variation across the tested grid, but a broader search might identify settings that improve performance on other cancer types or data configurations. Parametric alternatives such as iCluster [Shen et al., 2009] and Multi-Omics Factor Analysis (MOFA) [Argelaguet et al., 2018], which impose explicit latent structures across modalities, represent complementary directions for future comparison, particularly at higher event counts where their additional modelling assumptions may confer a precision advantage over non-parametric graph fusion. Fifth, the analysis uses segment-level GISTIC2 copy number, which aggregates large genomic regions; gene-level allele-specific copy number or focal amplitude scores might better distinguish subtypes that differ by discrete focal events rather than broad arm-level changes.

Taken together, the results suggest that SNF is a well-calibrated integration method for this problem: it consistently outperforms the weakest unimodal approaches and feature concatenation, and it produces a biologically coherent partition that independent IHC data confirm. The gap over the strongest single modality exists but is not yet statistically conclusive, and quantifying it properly requires a cohort with a substantially higher event count.

5 Conclusion

We benchmarked Similarity Network Fusion against four alternative multi-omics integration strategies on 644 TCGA-BRCA patients with matched RNA-seq, DNA methylation, and copy number profiles. SNF recovered PAM50 molecular subtypes more faithfully than RNA-seq alone (NMI $= 0.495$ vs 0.428) and substantially better than early feature concatenation (0.175), while producing a perfectly stable two-cluster partition independently confirmed by IHC receptor status. For survival prediction, SNF significantly outperformed CNV-only and a concatenation-based late-integration baseline; the advantage over RNA-seq alone was positive in direction but the bootstrap confidence interval included zero, an outcome that reflects the cohort's short follow-up and low event count rather than the absence of any true effect.

The practical implication is straightforward. SNF is worth using when multiple molecular layers are available: it consistently does better than dropping all but the most informative modality, and it does substantially better than stacking features naively. Whether the marginal gain over the best single modality justifies the added data collection cost will depend on the specific clinical context and on whether follow-up is long enough to detect the expected difference. Future work should test these findings in cohorts with longer follow-up, higher event rates, and treated populations where the multi-omic signal may translate more directly into treatment decisions.

Acknowledgements

We used TCGA-BRCA data made available through the NCI Genomic Data Commons under controlled access. PAM50 labels were obtained from the TCGA PanCanAtlas resource. No external funding is reported for this work.

References

R. Argelaguet, B. Velten, D. Arnol, S. Dietrich, T. Zenz, J. C. Marioni, F. Buettner, W. Huber, and O. Stegle. Multi-Omics Factor Analysis—a framework for unsupervised integration of multi-omics data sets. *Molecular Systems Biology*, 14(6):e8124, 2018. doi: 10.15252/msb.20178124.

Cancer Genome Atlas Network. Comprehensive molecular portraits of human breast tumours. *Nature*, 490(7418):61–70, 2012. doi: 10.1038/nature11412.

C. Curtis, S. P. Shah, S.-F. Chin, G. Turashvili, O. M. Rueda, M. J. Dunning, D. Speed, A. G. Lynch, S. Samarajiwa, Y. Yuan, et al. The genomic and transcriptomic architecture of 2,000 breast tumours reveals novel subgroups. *Nature*, 486(7403):346–352, 2012. doi: 10.1038/nature10983.

F. E. Harrell, R. M. Califf, D. B. Pryor, K. L. Lee, and R. A. Rosati. Evaluating the yield of medical tests. *JAMA*, 247(18):2543–2546, 1982. doi: 10.1001/jama.1982.03320430047030.

K. A. Hoadley, C. Yau, T. Hinoue, D. M. Wolf, A. J. Lazar, E. Drill, R. Shen, A. M. Taylor, A. D. Cherniack, V. Thorsson, R. Akbani, R. Bowlby, C. K. Wong, M. Wiznerowicz, F. Sanchez-Vega, A. G. Robertson, B. G. Schneider, M. S. Lawrence, H. Noushmehr, T. M. Malta, Cancer Genome Atlas Network, J. M. Stuart, C. C. Benz, and P. W. Laird. Cell-of-origin patterns dominate the molecular classification of 10,000 tumors from 33 types of cancer. *Cell*, 173 (2):291–304.e6, 2018. doi: 10.1016/j.cell.2018.03.022.

L. Hubert and P. Arabie. Comparing partitions. *Journal of Classification*, 2(1):193–218, 1985. doi: 10.1007/BF01908075.

R. D. Markello. snfpy: a Python package for Similarity Network Fusion. https://github.com/rmarkello/snfpy, 2019. Version 0.2.2.

J. S. Parker, M. Mullins, M. C. U. Cheang, S. Leung, D. Voduc, T. Vickery, S. Davies, C. Fauron, X. He, Z. Hu, J. F. Quackenbush, I. J. Stijleman, J. Palazzo, J. S. Marron, A. B. Nobel, E. Mardis, T. O. Nielsen, M. J. Ellis, C. M. Perou, and P. S. Bernard. Supervised risk predictor

of breast cancer based on intrinsic subtypes. *Journal of Clinical Oncology*, 27(8):1160–1167, 2009. doi: 10.1200/JCO.2008.18.1370.

C. M. Perou, T. Sørlie, M. B. Eisen, M. van de Rijn, S. S. Jeffrey, C. A. Rees, J. R. Pollack, D. T. Ross, H. Johnsen, L. A. Akslen, Ø. Fluge, A. Pergamenschikov, C. Williams, S. X. Zhu, P. E. Lønning, A.-L. Børresen-Dale, P. O. Brown, and D. Botstein. Molecular portraits of human breast tumours. *Nature*, 406(6797):747–752, 2000. doi: 10.1038/35021093.

S. Pölsterl. scikit-survival: A library for time-to-event analysis built on top of scikit-learn. *Journal of Machine Learning Research*, 21(212):1–6, 2020. URL http://jmlr.org/papers/v21/20-729.html.

N. Rappoport and R. Shamir. Multi-omic and multi-view clustering algorithms: review and cancer benchmark. *Nucleic Acids Research*, 46(20):10546–10562, 2018. doi: 10.1093/nar/gky889.

R. Shen, A. B. Olshen, and M. Ladanyi. Integrative clustering of multiple genomic data types using a joint latent variable model with application to breast and lung cancer subtype analysis. *Bioinformatics*, 25(22):2906–2912, 2009. doi: 10.1093/bioinformatics/btp543.

T. Sørlie, C. M. Perou, R. Tibshirani, T. Aas, S. Geisler, H. Johnsen, T. Hastie, M. B. Eisen, M. van de Rijn, S. S. Jeffrey, T. Thorsen, H. Quist, J. C. Matese, P. O. Brown, D. Botstein, P. E. Lønning, and A.-L. Børresen-Dale. Gene expression patterns of breast carcinomas distinguish tumor subclasses with clinical implications. *Proceedings of the National Academy of Sciences*, 98(19):10869–10874, 2001. doi: 10.1073/pnas.191367098.

B. Wang, A. M. Mezlini, F. Demir, M. Fiume, Z. Tu, M. Brudno, B. Haibe-Kains, and A. Goldenberg. Similarity network fusion for aggregating data types and finding patient and disease groups. *Nature Methods*, 11(3):333–337, 2014. doi: 10.1038/nmeth.2810.

W. Zhou, P. W. Laird, and H. Shen. Comprehensive characterization, annotation and innovative use of Infinium DNA methylation ProbeType designations. *Epigenetics & Chromatin*, 9(1): 37, 2016. doi: 10.1186/s13072-016-0087-z. Cited as Zhou2017; probe annotation resource for hg38 450k masking.